Electrochemistry of 6-Nitro-1′,3′,3′-trimethylspiro[2*H*-1-benzopyran-2,2′-indoline] Associated with Zeolite Y and MCM-41 Silicates. Light-Driven Site-Selective Electrocatalytic Effect on *N*,*N*,*N*′,*N*′,-Tetramethylbenzidine Oxidation

Antonio Doménech,*,† Hermenegildo García,‡ Isabel Casades,‡ and Mercedes Esplá‡

Departamento de Química Analítica, Universidad de Valencia, Dr. Moliner 50, Burjassot (Valencia), 46100, Spain, and Instituto de Tecnología Química UPV-CSIC, Universidad Politécnica de Valencia, Aptdo. 22012, 46071 Valencia, Spain

Received: July 16, 2004; In Final Form: September 30, 2004

The electrochemical response of open/closed forms of 6-nitro-1′,3′,3′-trimethylspiro[2*H*-1-benzopyran-2,2′-indoline] (**SP**) associated with zeolite Y (**SP@Y**) and MCM-41 silicates with or without framework Al (**SP@AlMCM** and **SP@MCM**, respectively) is described upon immersion of zeolite-modified polymer film electrodes into MeCN using $LiClO_4$, Et_4NClO_4, and Bu_4NPF_6 as supporting electrolytes. These samples show a reverse photochemical behavior, the open form undergoing ring closure to the closed one upon illumination with visible light ($\lambda > 450$ nm). Oxidation processes at +1.10 and +0.80 V vs AgCl (3 M NaCl)/Ag, corresponding to open and closed **SP**, respectively, exhibit a significant reversibility, suggesting that post-electron-transfer reactions resulting in the apparently irreversible voltammetry observed in solution are highly hindered here. Reduction of all boundary-associated **SP** forms occurs in two reversible one-electron steps involving the nitrobenzene group. Upon irradiation, **SP@Y** shows a remarkable site-selective electrocatalytic effect on the oxidation of *N*,*N*,*N*′,*N*′-tetramethylbenzidine (TMB) in Et_4NClO_4 and $LiClO_4$ electrolytes. Rotating disk voltammetry indicates that the rate-determining step can be attributed to the formation of a surface adduct between TMB and closed **SP** associated with the zeolite boundary. The value of the second-order rate constant of this process is 2.2×10^5 L/(mol s) in 0.10 M Et_4NClO_4/MeCN.

1. Introduction

The photochromism of spiropyrans was first reported by Fischer and Hirshberg in 1952.[1] Since then, these compounds have been studied extensively because of the wealth of possible applications in a variety of fields, including displays, information storage, and sensors.[2] Spiropyrans are composed of an indoline and a chromene moiety that are linked by a spirocarbon atom. In solution, irradiation with near-UV light ($\lambda < 350$ nm) induces heterolytic cleavage of the spiro-carbon−oxygen bond of the original closed spiropyran to produce a ring-opened species. In the absence of UV irradiation, this undergoes ring closure to re-form the parent spiropyran.

The reversible photochromism of spiropyranes is of interest for switching systems and transduction. Although the quantum efficiency of the light-activated ring opening and/or the thermal or light-driven ring closure limits the switching efficiency of the system,[3] the combination of photochemistry and electrochemistry offers possibilities for solving these drawbacks. Thus, immobilization of spiropyrans in self-assembled monolayers,[4,5] ionic Langmuir−Blodgett films,[6] and poly(Me methacrylate) matrix[7] has been recently described. Organization of a photoactivated command layer on an electrode can be used to control interfacial electron transfer and might be applied for the electronic transduction of optical signals.[8]

Accordingly, the electrochemistry of spiropyrans in solution has attracted attention in the last years. Thus, Campredon et al. obtained that reduction of nitro-functionalized spiropyrans in an aprotic environment leads to a stable radical species, while oxidations are electrochemically irreversible.[9] Fujishima et al. described the reduction of 8-nitro-1′,3′,3′-trimethylspiro[2*H*-1-benzopyran-2,2′-indoline] as a reversible electron-transfer process followed by a chemical reaction.[10−12] More recently, Preigh et al.[3] described the anodic oxidation mechanism of 6-hydroxy-1′,3′,3′-trimethylspiro[2*H*-1-benzopyran-2,2′-indoline] in terms of electron-transfer steps coupled with disproportionation, proton transfer, and dimerization reactions, thus resulting in an overall nonreversible behavior.

Because photoelectrochemical reversibility is desired for signal transduction, a possible strategy for improving the switching efficiency of spiropyrans is the insertion of activating/deactivating groups. Quantum chemistry calculations on the effect of substituents indicated that the presence of different deactivating groups on the indoline ring system and deactivating groups on the pyran system increases the ionization potential and, consequently, the oxidation potential.[13] However, chemical reactions coupled with electron-transfer processes may result in an apparent irreversibility.

In this context, immobilization of spiropyrans inside the rigid matrix of microporous and mesoporous aluminosilicates can be considered as a potentially interesting strategy for enhancing the switching efficiency of spiropyrans. In these hybrid organic−inorganic materials, the chemical properties of the guest are modulated by confinement effect, charge selectivity, and size selectivity provided by the host. The structure of crystalline aluminosilicates, such as zeolites, and MCM-41 defines channels and cavities of molecular dimensions in which molecules can

* Corresponding author. E-mail: antonio.domenech@uv.es.
† Universidad de Valencia.
‡ Universidad Politécnica de Valencia.

10.1021/jp046832r CCC: $27.50 © 2004 American Chemical Society
Published on Web 11/23/2004

be trapped. Encapsulation and isolation of individual molecules into microporous solids may block undesired reactions and increase the stability of reactive species.[14] Confinement of elusive organic cation guests into the rigid framework of zeolites produces a remarkable increase of the persistence of these reactive species when there is a tight fit of the guest inside the restricted reaction cavity defined by the host.[15,16]

Because post-electron-transfer reactions occurring in solution must be significantly hindered upon isolation of spiropyrans into the inorganic matrix, the electrochemistry of aluminosilicate-associated spiropyrans may exhibit a reversible behavior, thus increasing the switching efficiency of the system. The electrochemistry of zeolite-associated species has been widely studied in past decades.[17,18] Although some controversy concerning the detailed electrochemical mechanism exists,[19−22] it appears that the observed electrochemical response reflects essentially the behavior of extrazeolite ion-exchanged molecules and/or those located in the more external boundary layer of the zeolite.[23] In this context, Bessel and Rolison have developed the idea that different electrochemical redox isomers may be responsible for the observed electrochemistry,[23] using a terminology analogous to that proposed by Turro and García-Garibay in the study of zeolite-associated photochemical probes.[24] Subsequent data on the electrochemistry of zeolite-associated transition metal complexes[25] and reactive organic intermediates[26−28] provided results in agreement with such ideas. However, it appears that more detailed data on the existence of a site-characteristic electrochemistry are needed.

In the current work, we describe the electrochemical response of 6-nitro-spiropyran encapsulated into different silicates using sample-modified polymer film electrodes (PFEs) deposited over glassy carbon and platinum electrodes. For this study, we have used 6-nitro-1′,3′,3′-trimethylspiro[2*H*-1-benzopyran-2,2′-indoline] (**SP**) as a guest incorporated inside a tridirectional large pore zeolite Y (**SP@Y**) or adsorbed into mesoporous MCM-41 silicate with or without framework Al (**SP@AlMCM** and **SP@MCM**, respectively). In previous works, we have provided spectroscopic data of these samples showing the existence of a reverse photochemical behavior in which, under illumination with visible light ($\lambda > 450$ nm), the predominant open form undergoes ring closure to the closed spiropyran form. In addition, a third form consisting of protonated open spiropyran is also detected in the solids.[29,30] Thus, there is a distribution of three different species (closed, unprotonated open, and protonated open forms) whose population varies depending on the polarity and acidity of the solid, the open protonated form being the predominant species in the solids.[29,30]

Molecular modelizations indicate that both closed and open spiropyran molecules can be accommodated into zeolite Y supercages (diameter 1.4 nm) only through a ship-in-a-bottle synthesis because the **SP** molecule cannot cross the cage windows (diameter 0.74 nm). In contrast, MCM-41 silicates provide large pores (mean diameter ca. 3.2 nm) enabling for the ingress of spiropyran molecules into the pore/channel system. Because electron-transfer processes involving electroactive species associated with microporous materials involve the ingress/issue of electrolyte countercations to maintain charge neutrality,[17,18] the electrochemistry of **SP@Y** and **SP@MCM** materials may differ depending on their ability for interchanging electrolyte cations. Accordingly, and attempting to reflect possible differences in the electrochemical response of boundary-associated spiropyran molecules and mobile spiropyran molecules in the solution phase, voltammetric experiments on coatings of those materials immobilized into polymer film electrodes (PFEs) have been performed in $LiClO_4$/MeCN, Et_4NClO_4/MeCN, and Bu_4NPF_6/MeCN electrolytes.

In view of the insulating character of aluminosilicate materials, charging effects can distort seriously the voltammetric response of sample-modified electrodes. Attempting to avoid this problem, square wave voltammetry (SQWV) has been used because of its inherently high sensitivity and its immunity to capacitive effects.[31] To verify the existence of mass changes associated with electron-transfer processes, complementary electrochemical quartz-crystal microbalance (EQCM) experiments were performed.

The reactivity of zeolite-associated species has been widely studied in the past decade. As described by Yoon et al., the reactivity of zeolite-associated species is conditioned by the size and shape selectivity of cations in mediating electron-transfer processes.[32] Interaction between entrapped molecules[33] and their distribution in the zeolite microcrystals[34] can also influence the observed reactivity. As was recently pointed out by Rolison and Bessel on reviewing charge-transfer reactions at redox-modified zeolites,[35] it is pertinent to determine the extent of a topological control of the reactivity in such systems.

Attempting to explore the capabilities of zeolite-associated spiropyrans for promoting electron-transfer reactions, the electrocatalytic effect of **SP@Y**, **SP@MCM**, and **SP@AlMCM** on the oxidation of *N*,*N*,*N*′,*N*′-tetramethylbenzidine (TMB) has been studied. This compound provides a well-known reversible electrochemical behavior that could be sensitive to reactions with spiropyrans. Additionally, because different topological redox isomers may be involved in electrochemical reactions of zeolite-associated species, electrocatalytic processes may reflect site-depending effects. Prior data on the electrocatalysis of 1,4-dihydrobenzoquinone oxidation by a mesoporous organosilica material containing 4,4′-bipyridinium units covalently attached to a MCM-41 matrix act in support of that idea.[36] Site-selective electrocatalytic effects are potentially interesting for developing highly selective electrochemical sensors and/or electrosynthetic routes.

2. Experimental Section

2.1. Materials and Chemicals. SP@Y (Si/Al ratio 2.4) was obtained by ship-in-a-bottle synthesis by stirring at reflux temperature a suspension of dehydrated NaY in ethanol containing equivalent amounts of 2-methylene-1,3,3-trimethyl-indoleine and 2-hydroxy-5-nitrobenzaldehyde in ethanol.[29]

SP@AlMCM (MCM-41, Si/Al = 15) and **SP@MCM** (MCM-41, Si/Al = ∞) were prepared by adsorbing preformed **SP** onto dehydrated mesoporous samples (pore size 3.2 nm) as was reported in detail elsewhere.[30] Zeolite NaY (P.Q. Industries), 2-methylene-1,3,3-trimethylindoline (Aldrich), and 2-hydroxy-5-nitrobenzaldehide (Aldrich) were commercial samples and used as received. A similar procedure was followed for adsorbing **SP** onto silica and alumina.

The corresponding AlMCM and MCM silicates were obtained by hydrothermal crystallization at 80 °C for 3 days using tetraethoxysilane (TEOS) and Al_2O_3 as sources and ethyltrimethylammonium bromide as structure-directing agent as was previously reported.[37] The synthesis of the siropyran-supported materials was carried out by stirring a suspension of the zeolite in an equimolecular mixture of indoline and the corresponding benzaldehyde in CH_2Cl_2 under reflux conditions for 7 days. To remove unreacted starting materials, exhaustive solid−liquid extraction with a micro-Soxhlet apparatus with ethanol as the solvent was routinely used. The materials were eventually stirred 48 h in a 1 M NaCl aqueous solution to remove guest molecules

located in external defect sites. These are referred to in the following as NaCl-treated materials. Spectrometric data and elemental analysis[29,30] indicated that spiropyran molecules with negligible secondary products were synthesized into the zeolite Y and MCM silicates. The amount of encapsulated **SP** was 1.14 $\times$ 10^{-7} and 1.22 $\times$ 10^{-7} mol of **SP**/mg of material for **SP@Y** and **SP@MCM** (and **SP@AlMCM**), respectively.

The materials were stored under dark conditions before use, and the modified electrodes were prepared in a dark chamber. Irradiation of the solid powders was carried out using an Oriel photoreactor adapted with a 420−630 nm dichroic filter (Oriel part#66219). Prior to electrochemical experiments, a fine spot of ca. 200 mg of the materials deposited on a glass surface was irradiated with a conventional 120 W/220 V lamp during a period of 48 h. At the end of that process, the UV−vis spectrum changed entirely from the original open spiropyran to that of its closed form, as was described previously (see Supporting Information).[28,29] Modified electrodes were prepared from pristine "dark" materials and "bleached" samples after 24 and 48 h of irradiation.

2.2. Modified Electrode Preparation. Sample-modified polymer film electrodes were prepared on the basis of the methods devised by Bessel and Rolison,[23] and Calzaferri et al.[38] Paraloid B72, an ethyl methacrylate (70%)−methyl acrylate (30%) copolymer (P[EMA/MA]), was selected for PFE preparation because of its ability to form uniform thin films, insolubility in water, and chemical and mechanical stability.

As was previously described,[24] a few microliters (typically 50 μL) of a dispersion of the solid (10 mg) in acetone (5 mL) was transferred to the surface of the glassy carbon or platinum electrode, and the coating was allowed to dry in air. After the electrode surface was air-dried, one drop of a solution of the acrylic resin (1%) in acetone was added and the modified electrode was air-dried. The coatings examined contained 0.2−1.5 mg/cm^2 of the dry material.

Paraffin-impregnated graphite electrodes (PIGEs), developed by Scholz et al.,[39] have been extensively used in past years for studying the electrochemical behavior of solid materials. PIGEs consist of cylindrical rods of diameter 5 mm of graphite impregnated under vacuum by paraffin. Preparation details are described in ref 39. These electrodes facilitate the direct contact between the zeolite particles and the substrate electrode, which is a crucial aspect for studying the electrochemistry of zeolite-associated species.[19−23] Modified PIGEs provide large currents and high stability in repetitive voltammetric experiments as reported elsewhere.[36]

To prepare modified paraffin-impregnated graphite electrodes, 0.10−0.50 mg of sample was placed on a glazed porcelain tile forming a spot of finely distributed material. The lower end of the graphite electrode was then gently rubbed over that spot of sample and finally cleaned with a tissue paper to remove ill-adhered particles.

2.3. Instrumentation and Procedures. Molecular modelizations were performed with the molecular mechanics Discover 3.1 program package as was already described.[28,29] Linear potential scans (LSVs), cyclic voltammograms (CVs), and square wave voltammograms (SQWVs) were performed with a BAS CV50W equipment. A standard three-electrode arrangement was used with a platinum auxiliary electrode and a AgCl (3 M NaCl)/Ag reference electrode in a thermostated cell. For experiments in MeCN, the reference electrode was separated from the solution using a capillary salt bridge. As working electrodes, glassy carbon (BAS MF 2012, geometrical area 0.071 cm^2) and platinum (BAS MF 2013, geometrical area 0.017 cm^2) electrodes were used. Prior to the series of runs, the reference electrode was calibrated with respect to the ferricinium/ferrocene couple in 0.10 M Bu_4NPF_6/MeCN.

Rotating disk voltammetry was carried out with a Metrohm 628-10 assembly. Microgravimetric experiments were performed on a CH I420 electrochemical quartz crystal microbalance (EQCM) incorporating a gold-coated AT-cut quartz crystal. The quartz crystal and gold electrodes had diameters of 1.20 and 0.50 cm, respectively. The reference and counter electrodes were the same as in voltammetric studies. The EQCM instrument was calibrated via electrochemical deposition of copper from 1.0 mM $Cu(ClO_4)_2$ + 0.10 M $HClO_4$ following the procedure described by Deakin and Melroy.[40] Electrogravimetric experiments were performed after deposition of ca. 1 mg of zeolite on the gold electrode from an acetone suspension of that material. Assumptions made for using the Sauerbrey equation to determine mass changes were as described by Bond et al.[41]

To study possible leaching/ion exchange effects, a series of electrochemical experiments were performed after magnetic stirring of suspensions (100 mg/L) of the materials at 600 rpm in each one of the electrolytes for 2 h under dark conditions. Voltammograms were recorded at bare glassy carbon and Pt electrodes under quiescent conditions in the filtered solution. In the following, we refer to the resulting solutions as "stirred solutions".

Electrocatalytic experiments were performed in 0.0−5.0 mM solutions of *N*,*N*,*N*′,*N*′-tetramethylbenzidine (TMB) in different MeCN electrolytes using paraffin-impregnated graphite electrodes (PIGEs). Photochronoamperometric experiments were performed by applying a constant potential of +1.0 V upon time-controlled irradiation of the working electrode with a conventional lamp (220 V/100 W).

To avoid the possible influence of impurities in aluminosilicates, blank electrochemical and photoelectrochemical experiments were also carried out for pristine (non **SP**-containing) zeolite Y and MCM-41.

Experiments were conducted in MeCN using $LiClO_4$ (Aldrich), Et_4NClO_4 (Acros), and Bu_4NPF_6 (Fluka) electrolytes. All electrochemical measurements were performed in well-deaerated solutions under an atmosphere of argon.

3. Results and Discussion

3.1. Electrochemistry of SP@MCM and SP@AlMCM. In Figure 1, the CVs of **SP@MCM** deposited on a GCE and immersed into (a) 0.10 M Et_4NClO_4/MeCN and (b) 0.10 M Bu_4NPF_6/MeCN, under dark conditions, are shown. Despite large background currents, a main oxidation peak at +1.1 V appears in initial anodic scan CVs. This peak exhibits a weak cathodic counterpart at +1.0 V and is accompanied by overlapped cathodic peaks near +0.50, −0.80, and −1.0 V, whose anodic counterparts are extremely weak, and ill-defined anodic peaks at +0.6 and +0.8 V. These peaks are accompanied by an ill-defined couple near 0.0 V (marked by * in Figure 1). This couple is recorded in blank CVs performed at unmodified glassy carbon electrodes (see Figure 1c), being attributable, following literature,[42,43] to the reduction/oxidation of surface-bound species which have been associated with quinone/hydroquinone functionalities on carbon electrodes.

Because commercial silicates can contain significant levels of impurities (iron, chloride, etc.), eventually affecting their electrochemical response, blank experiments were performed using electrodes modified with pristine MCM-41. The voltam-

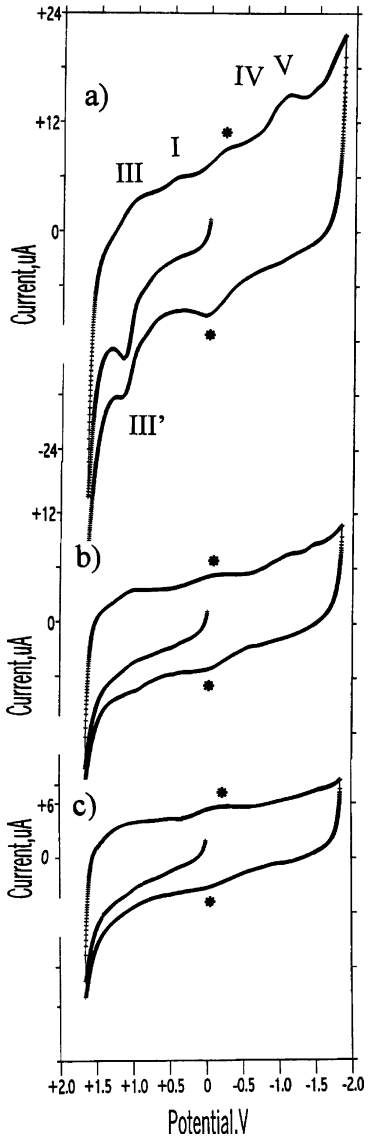

Figure 1. CVs of **SP@MCM** deposited on GCE immersed in (a) 0.10 M Et_4NClO_4/MeCN; (b) 0.10 M Bu_4NPF_6/MeCN. (c) CV recorded at an unmodified GCE immersed into 0.10 M Et_4NClO_4/MeCN. All experiments were performed under dark conditions. Potential scan rate 100 mV/s.

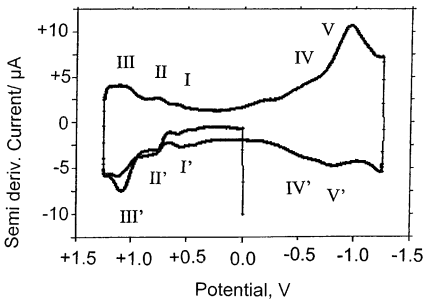

Figure 2. CV after semiderivative convolution of a **SP@MCM**-modified PFE immersed into 0.10 M $LiClO_4$/MeCN under dark conditions. Potential scan rate 100 mV/s.

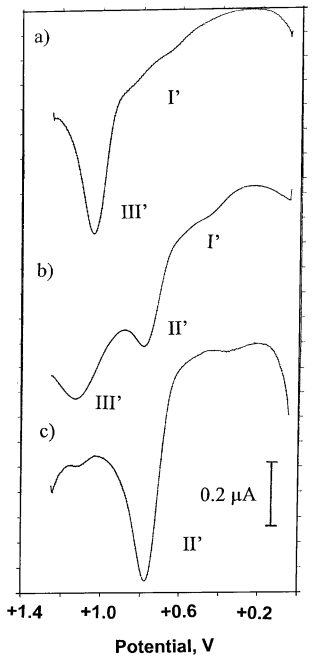

Figure 3. SQWVs of **SP@AlMCM**-modified GCEs in 0.10 M Et_4NClO_4/MeCN. Pristine sample (a) under dark conditions, (b) at an intermediate stage of bleaching, and (c) after complete bleaching (see details in Experimental Section). Potential scan initiated at +0.05 V in the positive direction. Potential step increment 4 mV; square wave amplitude 25 mV; frequency 15 Hz.

metric response was almost identical to that recorded at unmodified GCEs.

The peaks recorded for **SP@MCM** in contact with $LiClO_4$/MeCN and Et_4NClO_4/MeCN are clearly larger than those in contact with Bu_4NPF_6/MeCN, as is expected as a result of the ability of Li^+ and Et_4N^+ ions to be zeolite-exchanged. A similar result was obtained for CVs recorded on **SP@AlMCM**.

Upon convolution, CVs exhibit a well-defined profile, as illustrated in Figure 2 for **SP@MCM** in contact with $LiClO_4$/MeCN. In the initial anodic scan, a weak oxidation peak appears at +0.6 V (I′) followed by overlapped peaks at +0.85 (II′) and +1.17 V (III′). In the subsequent cathodic scan, reduction peaks at +1.08 (III), +0.78 (II), and +0.55 V (I) appear, followed by reduction peaks at −0.50 (IV) and −1.10 V (V). These last are associated with anodic peaks at −0.8 (V′) and −0.4 V (IV′). Interestingly, cathodic and anodic peaks display similar profiles, thus defining apparently reversible couples I/I′, II/II′, III/III′, IV/IV′, and V/V′. As further discussed, peaks I′−III′ can be described in terms of the oxidation of different closed and open spiropyran forms to radical cation derivatives, whereas peaks IV and V correspond to the reduction of such spiropyran forms to the corresponding radical anions (vide infra).

The amount of electroactive **SP** can be estimated using Faraday's law by integrating the quantities of charge passed under the voltammetric peaks. For modified electrodes containing 0.25 mg of modifier, net amounts of charge of 3 μC passed. Because the total spiropyran concentration into the materials was 1.2×10^{-7} mol **SP**/mg material, one finds that only 0.10% of the encapsulated **SP** was electroactive.

As was previously described,[29,30] after irradiation, the materials undergo a bleaching process as a result of the cyclization of open spiropyran molecules. The electrochemistry of samples during different stages of the bleaching process is illustrated in Figure 3 for **SP@AlMCM** in 0.10 M Et_4NClO_4/MeCN. In this figure, the SQWVs of the dark conditioned material before (Figure 3a) and after intermediate (Figure 3b) and complete bleaching (Figure 3c) are shown. As expected, SQWVs reduced capacitive effects and provided well-resolved peaks. Upon bleaching, peak III′ decreases and is lightly shifted toward more positive potentials while being progressively replaced by peak II′. Weak overlapping peaks at ca. +0.5 V (I′) also appear in SQWVs. Upon bleaching, such peaks are shifted to potentials

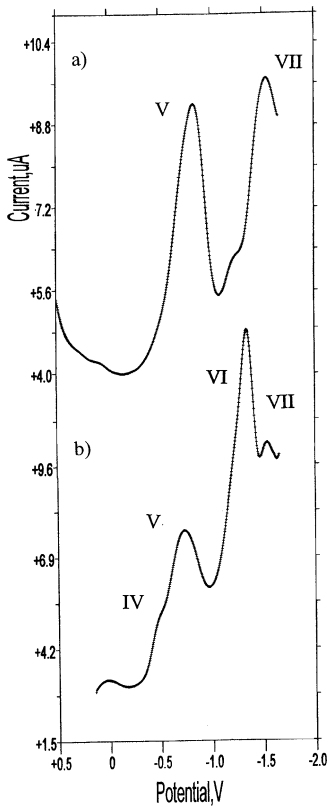

Figure 4. SQWVs of **SP@MCM** in 0.10 M Et_4NClO_4/MeCN: (a) under dark conditions, and (b) after irradiation. Potential scan initiated at +0.15 V in the negative direction. Potential step increment 4 mV; square wave amplitude 25 mV; frequency 5 Hz.

of ca. +0.4 V. Similar results are obtained when the bleaching process is followed by cathodic SQWVs, with peak II enhanced progressively at the expense of peak III (see Supporting Information). A similar response is obtained using 0.10 M $LiClO_4$ and Bu_4NPF_6 as supporting electrolytes, but in this last case the peaks are significantly decreased in agreement with CV data (see Figure 1).

On scanning the potential in the +0.15/−1.65 V potential region, SQWVs of **SP@MCM** and **SP@AlMCM** under dark conditions are almost identical in all electrolyte media. As depicted in Figure 4, well-defined peaks at −0.85 (V) and −1.58 V (VII) preceded by ill-defined shoulders near −0.55 (IV) and −1.32 V (VI) appear. After bleaching of zeolite samples by irradiation with visible light, peaks IV and VI are enhanced while peaks V and VII decrease as can be seen in Figure 4b.

The observed results exhibit a close similarity, but also significant differences from those reported for spiropyrans in solution. On first examination, the electrochemistry of **SP@MCM** and **SP@AlMCM** in all tested electrolyte media can be described in terms of oxidation processes for closed (process II′) and open (process III′) spiropyran forms, taking into account the reverse photochemical behavior observed for spiropyrans adsorbed in zeolites or aluminosilicates. Remarkably, cathodic peaks II and III appear in the voltammetry of such spiropyran-containing materials, while these peaks are entirely absent in the response of spiropyrans in solution.

Thus, the electrochemical oxidation of the closed nitrospiropyrans in solution consists of two irreversible processes near +0.8 and +1.1 V.[10−12] This parallels the electrochemical behavior of 6-hydroxy-1′,3′,3′-trimethylspiro[2*H*-1-benzopyran-2,2′-indoline], described by Freigh et al.[3] in terms of an initial oxidation of the indolene moiety to a radical cation further converted to a open semiquinone radical which disproportionates into a quinone and a hydroquinone, the last being oxidized to quinone at higher electrode potentials. The intermediate semiquinone radical dimerizes, thus avoiding the appearance of coupled cathodic peaks.[3]

SCHEME 1: Scheme of Electrochemical Processes Involved in the Oxidation of Closed and Open Spiropyrans in Solution

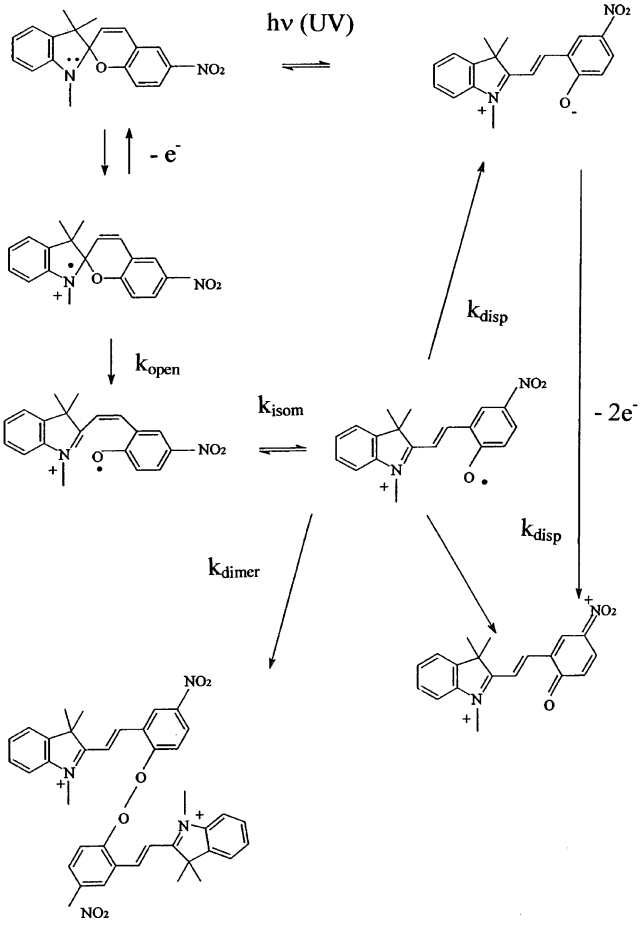

A reaction scheme is depicted in Scheme 1 in which, following Flannery,[42] open **SP** is represented by its zwitterionic form rather than by the merocyanine form. The occurrence of fast chemical reactions following electron-transfer steps, however, blocks the appearance of cathodic peaks in experiments performed for spiropyrans in the solution phase.[3,10−12] As a result, an apparently irreversible response is observed in solution, consisting of two anodic peaks (corresponding to peaks labeled here as II′ and III′) without coupled cathodic signals.

A similar scheme can apply for nitrospiropyrans in MCM materials. Here, under dark conditions, the open **SP** form predominates and only one oxidation process III′ appears (Figure 3a). Upon irradiation, the open form is converted into the closed one and the oxidation process II′ increases at the expense of peak III′ (Figure 3b). Remarkably, after exhaustive irradiation, peak II′ replaces entirely the III′ peak as can be seen in Figure 3c. This contrasts with the response of closed **SP** in solution, in which peak III′ accompanies peak II′. This suggests that, when associated with MCM materials, the oxidation of the closed form yields closed oxidized forms rather than open oxidized ones. This means that the post-electron-transfer reactions of ring opening and a cis−trans isomerization reaction occurring in solution are significantly hindered for **SP@MCM** and **SP@AlMCM**.

Peaks I′ can be attributed to minority **SP** species existing in the aluminosilicate probably as a result of secondary isomerization reactions occurring during the synthesis of such materials. Peak broadening and peak potential shift of peak III′ (and peak I′) observed during the bleaching process can tentatively be attributed to the superpositions of the response of "free" and silicate-associated **SP**.

The electrochemical processes IV−VII can be attributed to the reversible reduction of the nitroaromatic moiety in two successive one-electron steps, in agreement with literature data.[9,44] Accordingly, peaks V and VII in Figure 4 can in principle be described as two successive one-electron-transfer processes involving the nitroaromatic moiety of open forms, while peaks IV and VI in those figures are attributable to similar electron-transfer processes affecting closed spiropyran molecules. In this context, the electrode processes I/I′ can be attributed to merocyanine derivatives resulting from the alteration of surface spiropyran molecules.

The picture depicted in Scheme 1 appears to be valid for spiropyran molecules passing to the electrolyte solution as a result of the facile ion exchange prompted by the large pore window MCM substrate. However, the appearance of weak cathodic peaks II and III suggests that any type of association with the inorganic host persists, thus resulting in a stabilization of the reactive cation intermediates produced in the oxidation processes II′ and III′.

3.2. Electrochemistry of SP@Y. The possible persistence of an organic guest−inorganic host association during electrochemical turnovers can be tested for **SP@Y** because in this material the relatively small pore diameter must make difficult or even block ion-exchange processes involving bulky species.

Thus, while the voltammetry of **SP@Y** recorded under dark conditions in $LiClO_4$/MeCN and Et_4NClO_4/MeCN electrolytes is close to that previously described for **SP@MCM** and **SP@AlMCM**, the electrochemistry in contact with Bu_4NP_6/MeCN is remarkably different. As can be seen in Figure 5a, in contact with Bu_4NPF_6/MeCN, **SP@Y** displays only one weak peak at +1.18 V (III′) with no coupled cathodic peaks. By contrast, upon immersion into Et_4NClO_4/MeCN (Figure 5b), the tall peak III′ at +1.18 V is accompanied by a cathodic counterpart III, and the peaks II/II′ (see also Supporting Information) that look like two superimposed couples near +0.80 and +0.74 V.

Upon repetitive voltammetry (see Figure 5c), the more prominent peak III′ decays rapidly. However, after 3−5 successive scans on the same modified electrode, a weak stationary response remains for several scans. Here, couple III/III′ looks like two overlapping couples at equilibrium potentials close to +1.10 V, whereas the couple II/II′ becomes a single pair of peaks at +0.74 V. The appearance of cathodic peaks II and III, peak splitting, and the decrease of the III′ peak at the expense of the II′ peak are features that are entirely absent for **SP** in the solution phase and adsorbed onto silica or alumina. The pertinent peak potential data are summarized in Table 1.

It is interesting to note that the voltammetric response of pristine **SP@Y** was identical to that of this material after being submitted to prolonged stirring forming a suspension in a 1 M NaCl aqueous solution. This is indicative, consistently with spectrochemical data, of the absence of significant release of **SP** from the zeolite via ion exchange. In contrast, the voltammetry of **SP** adsorbed onto silica or alumina was found to be identical to that recorded in solution.

The net amount of charge passed for **SP@Y**-modified electrodes in contact with Et_4NClO_4/MeCN and $LiClO_4$/MeCN

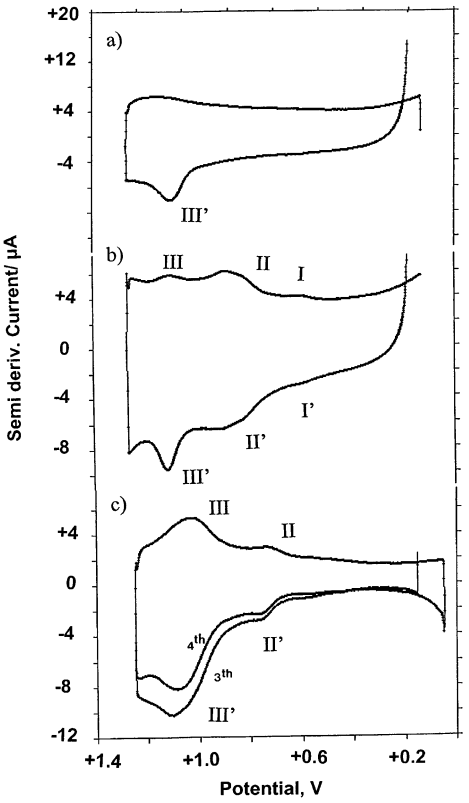

Figure 5. CVs under dark conditions, after convolution, of **SP@Y** deposited on Pt in contact with (a) 0.10 M Bu_4NPF_6/MeCN, first scan; (b) 0.10 M Et_4NClO_4/MeCN, first scan; (c) 0.10 M Et_4NClO_4/MeCN, third and fourth scans. Potential scan rate 100 mV/s.

TABLE 1: Peak Potential Data (mV vs AgCl (3 M NaCl)/Ag) in CVs of SP@Y-Modified Electrodes Immersed into $LiClO_4$/MeCN, Et_4NClO_4/MeCN, and Bu_4NPF_6/MeCN, All in 0.10 M Concentration[a]

		peak potentials (cathodic/anodic)	
electrolyte	conditions	couple III/III′ (mV)	couple II/II′ (mV)
Bu_4NPF_6/MeCN	first scan	−/+1070	
Bu_4NPF_6/MeCN	third scan	−/+1070	
Et_4NClO_4/MeCN	first scan	+1050/+1070	+810/+830, +745/+735
Et_4NClO_4/MeCN	third scan	+1040/+1045	+735/+770
$LiClO_4$/MeCN	first scan	+1100/+1080	+830/+840, +730/+750
$LiClO_4$/MeCN	third scan	+1070/+1080	+730/+740

[a] Values recorded, after convolution, from three independent measurements on modified electrodes under dark conditions. Potential scan rate 100 mV/s.

electrolytes was lower than that obtained for **SP@MCM** and **SP@AlMCM** materials. A 0.07% of the zeolite Y encapsulated **SP** was found to be electroactive. This result confirms the idea that the observed electrochemistry corresponds essentially to **SP** molecules located in the boundary sites of the zeolite grains.

As was previously described for MCM-41 materials, upon irradiation of **SP@Y** samples, the couple II/II′ replaces the pairs I/I′ and III/III′ (see Supporting Information). Under our experimental conditions, blank voltammetric experiments performed on pristine (noncontaining **SP**) zeolite Y provided responses similar to those of unmodified electrodes.

Attempting to discern the response of species in solution and zeolite-associated species, we recorded the voltammetric response at a bare Pt electrode of a quiescent solution resulting from stirring of a suspension of **SP@Y** in 0.10 M Bu_4NPF_6/

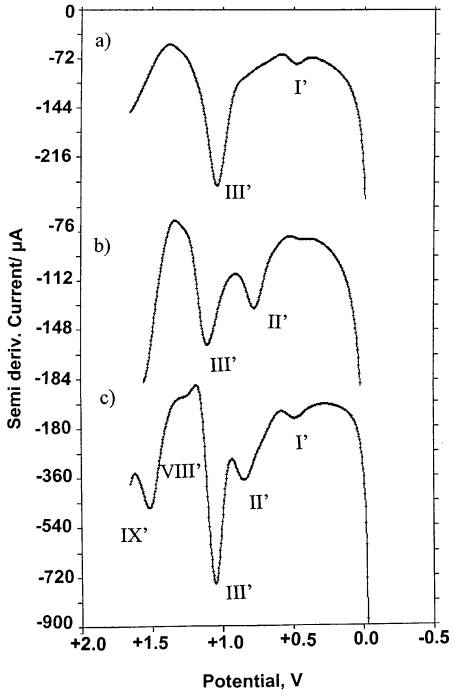

Figure 6. Semiderivative convolution of SQWVs recorded (a) at a Pt electrode immersed into a 0.10 M Bu_4NPF_6/MeCN after stirring of **SP@Y** (see details in Experimental Section); (b) in 0.10 M Et_4NClO_4/MeCN; and (c) a **SP@Y**-modified electrode immersed into 0.10 M Et_4NClO_4/MeCN. Potential step increment 4 mV; square wave amplitude 25 mV; frequency 5 Hz.

MeCN. The SQWV response of that resulting solution, consisting of peak III′ (and weak I′), is depicted in Figure 6a. This response equals that obtained for **SP@Y**-modified Pt electrodes immersed in 0.10 M Bu_4NPF_6/MeCN.

In contrast, after suspensions of **SP@Y** in 0.10 M Et_4NClO_4/MeCN were stirred, the response in the quiescent resulting solution consisting of separated peaks I′ (weak), II′, and III′ is obtained, as can be seen in Figure 6b. This response differs from that recorded for **SP@Y**-modified electrodes immersed in Et_4NClO_4/MeCN or $LiClO_4$/MeCN, depicted in Figure 6c. Here, the voltammetric profile becomes more complicated, with additional anodic peaks at +1.20 (VIII′) and +1.45 V (IX′). On repeating the potential scan, peak III′ decreases and peaks VIII′ and IX′ become well defined, as can be seen in Figure 7a, and they are accompanied by cathodic peaks VII and IX (see Figure 7b).

The concentration of SP in solutions resulting from the stirring of **SP@Y** suspensions was calculated from peak current measurements by comparison with peak currents measured in solutions of SP, from which the amount of **SP** leached from **SP@Y** in 0.10 M Et_4NClO_4/MeCN was estimated as 0.01−0.02% of the total amount of entrapped **SP**.

In the +0.15/−1.65 V potential range, SQWVs of **SP@Y** are again electrolyte-dependent, but similar are to those of **SP@MCM** and **SP@AlMCM** (see Supporting Information). On scanning the potential in the positive direction, the anodic counterparts of peaks IV−VII are recorded, suggesting that all of these electrode processes behave reversibly. For **SP@Y** in 0.10 M Et_4NClO_4 under dark conditions (see Figure 8a), peaks at −1.39 (VII′), −1.16 (VI′), −0.78 (V′), and −0.50 V (IV′) appear, the last being the most prominent in the region of negative potentials, whereas peaks I′, II′, and III′ appear at positive potentials. Upon irradiation, peaks IV and IV′ are enhanced in all cases at the expense of peaks V and V′ as can be seen in Figure 8b.

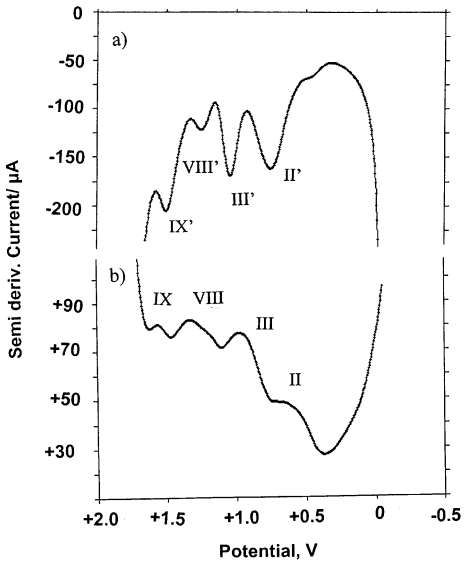

Figure 7. Semiderivative convolution of SQWVs (fifth scan) of PFEs modified by **SP@Y** immersed in 0.10 M Et_4NClO_4/MeCN. (a) Potential scan initiated at +1.65 V in the negative direction; and (b) initiated at −0.05 V in the positive direction. Potential step increment 4 mV; square wave amplitude 25 mV; frequency 5 Hz.

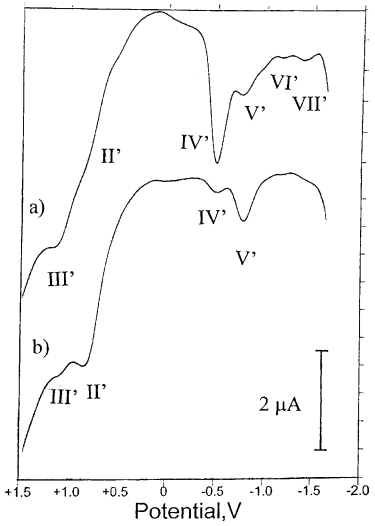

Figure 8. SQWVs of **SP@Y** in 0.10 M Et_4NClO_4/MeCN: (a) under dark conditions and (b) after irradiation with visible light. Potential scan initiated at −1.65 V in the positive direction. Potential step increment 4 mV; square wave amplitude 25 mV; frequency 15 Hz.

It should be noted that charge conservation implies that each electron-transfer process involving zeolite-associated species must necessarily be accompanied by the ingress/issue of a mobile cation in the zeolite pore/channel system from the solution phase.[17,18] Accordingly, the large pore size of MCM materials (3.2 nm) allows for an easy interchange of spiropyran molecules and all Li^+, Et_4N^+, and Bu_4N^+ cations (kinetic diameters of ca. 0.35, 0.75, and 1.25 nm, respectively) between the MCM matrix and the electrolyte solution. In contrast, zeolite Y (pore size 0.74 nm) is able to interchange Li^+ and Et_4N^+ ions with the adjacent electrolyte media, but not spiropyran molecules and bulky Bu_4N^+ ions.[45,46]

The electrochemistry of **SP@Y** can be described in terms of the superposition of the responses of at least three different redox isomers: (i) "free" spiropyran molecules existing in the solution phase as a result of the egress of externally adsorbed or occluded molecules; (ii) **SP** weakly associated with the zeolite boundary able to be ion-exchanged with the electrolyte cations that

produce a response controlled by diffusion of such ions in the zeolite system; and (iii) spiropyran molecules strongly associated with the zeolite boundary. The term zeolite boundary is used here to represent the external layer of zeolite crystals comprising their more external surface and the cavities close to that external surface.

With regard to spiropyran electrochemistry, one can expect that the response of "external" redox isomers (i) and (ii) equals that of spiropyrans (open and/or closed forms) in solution, characterized by an apparently irreversible oxidation profile. On the contrary, one can expect that redox isomers and (iii) (and, at least partly, redox isomers (ii)) inhibit post-electron-transfer dimerization reactions, thus providing a reversible electrochemistry.

In the case of **SP@MCM** and **SP@AlMCM**, because of the facile interchange of spiropyran molecules and electrolyte cations, the redox isomers (i) and (ii) must dominate the observed electrochemistry regardless of the electrolyte countercation.

For **SP@Y**, only external molecules resulting from breaking of external cages (isomer (i)) can produce the electrochemical response (peak III′ alone) observed in Bu_4NPF_6 electrolytes. The voltammetric profile (Figure 5a) then becomes irreversible as recorded in stirred solutions (Figure 6a). In $LiClO_4$/MeCN and Et_4NClO_4/MeCN electrolytes, however, all redox isomers can undergo electron-transfer processes, as was previously discussed for zeolite Y-associated Mn(salen)N_3,[25] and 2,4,6-triphenyl- pyrilium[27] and thiopyrylium ions.[28] As in these cases, the voltammetric response is initially dominated by a solution-like behavior, progressively changing under repetitive cycling of the potential scan. Thus, as is shown in Figure 5b,c, the initial irreversible two-electron pattern of peak III′, due to "external" open **SP**, prevails in the first scan. In successive scans, this peak evolves to a reversible one-electron profile attributable to boundary-associated **SP**. It should be emphasized that the voltammetry of **SP@Y** (but also of **SP@MCM** and **SP@AlMCM**) in $LiClO_4$/MeCN and Et_4NClO_4/MeCN electrolytes differs significantly from that described for spiropyrans in solution. Thus, the electrochemical processes II′ and III′ exhibit well-defined cathodic counterparts II and III (see Figures 2, 5b,c), denoting a reversible behavior. In contrast, experiments in solution do not provide peaks II and III.[10−12]

Accordingly, the couple II/II′ appears initially as two superimposed pairs of peaks at +0.80 and +0.74 V, attributable to "external" and "boundary-associated" redox isomers. Upon repetitive voltammetry, external **SP** diffuses to the bulk of the solution, and the voltammetric response is limited to that of the boundary-associated isomer. The pertinent peak potential data are summarized in Table 1. It can be seen that the cathodic to anodic peak potential separation, ΔE_p, is lower than the expected value for a one-electron reversible couple (59 mV). This suggests that the observed processes approaches a thin-layer behavior (for which $\Delta E_p = 0$), attributable to boundary-associated species.[25,28]

The appearance of this dual response can be interpreted in the light of the model developed by Lovric, Scholz, Oldham, and co-workers[47−50] for redox conductive microcrystals and the model of Andrieux and Savéant[51] for redox polymers. It is assumed that the reaction starts at the three-phase boundary between electrode, zeolite particle, and electrolyte. From this point, the reaction zone grows, while electrons and charge-balancing cations diffuse perpendicularly along the zeolite. As a result, at short times, a Cottrell-type behavior, controlled by the diffusion of electrolyte countercations in the zeolite, can be expected. At larger times, a thin-layer response in which electron

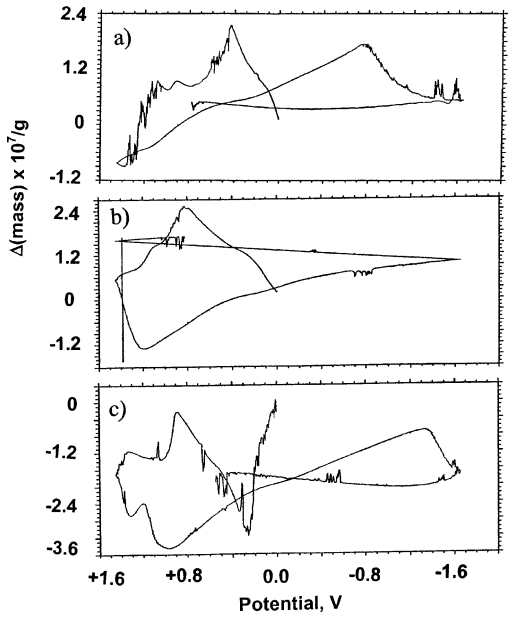

Figure 9. Mass increment/potential graphs obtained in EQCM experiments at (a) unmodified gold electrode immersed into 0.10 M Et_4NClO_4/MeCN; (b) **SP@Y**-modified electrode in contact with 0.10 M Bu_4NPF_6/MeCN; and (c) **SP@Y**-modified electrode in contact with 0.10 M Et_4NClO_4/MeCN. The potential was cycled between +1.45 and −1.65 V starting from 0.0 V. Potential scan rate 10 mV/s.

hopping between adjacent redox sites acts as a rate-controlling step should be operative. As was already described in detail,[52] this model can be applied to interpret the electrochemistry of zeolite-associated species.

Electrogravimetric experiments were performed on deposits of zeolite microsamples over the gold electrode of a EQCM, attempting to verify the existence of processes of ingress/issue of charge-balancing cations coupled with electron-transfer steps.

In Figure 9a, we depicted a typical mass change/potential graph for the unmodified gold electrode immersed in 0.10 M Et_4NClO_4/MeCN. Confirming voltammetric data, the response of **SP@Y**-modified electrodes is remarkably electrolyte-dependent. Thus, as shown in Figure 9b, in contact with 0.10 M Bu_4NPF_6/MeCN, the mass change response is essentially identical to that of the unmodified electrode. However, in contact with 0.10 M Et_4NClO_4/MeCN (Figure 9c), a significant mass loss occurs on scanning the potential in the positive direction from 0.0 V. The quotient mass loss/charge passed varied between 20 and 55 g/mol. These values are consistent with the stepwise oxidation of boundary-associated spiropyran molecules accompanied by the issue of one or two Na^+ ions from the zeolite to the electrolyte solution.

On assuming that zeolite encapsulation stabilizes the generated radical cations and blocks competing post-electron-transfer processes, disproportionation, cis−trans isomerization, and dimerization, the response in Figure 5c can be described in terms of successive reversible one-electron processes involving boundary-associated spiropyran molecules. Accordingly, the reversible processes II′ and III′ can be represented as:

$$\mathbf{SP}\ (b) + Na^+\ (b) \rightarrow \mathbf{SP}^{\bullet +}\ (b) + Na^+\ (s) + e^- \qquad (1)$$

where (b) represents the zeolite boundary and (s) is the solution phase.

A possible scheme for electrochemical processes involving boundary-associated closed and open spiropyran forms is presented in Scheme 2. On comparison with the solution-like Scheme 1, the relevant point to emphasize is that post-electron-

SCHEME 2: Summary of the Electrochemical Processes Involved in the Oxidation of Boundary-Associated SP@Y, SP@AlMCM, and SP@MCM Systems

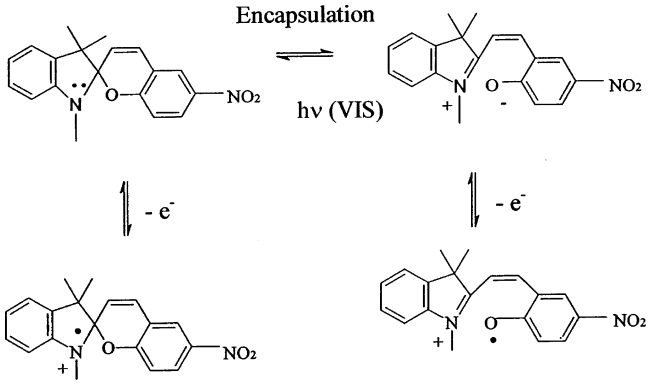

transfer reactions are inhibited because of the stability of the oxidation products in the inorganic host.

Due to the frozen orthogonal configuration of the indolic and phenolate moieties, the closed spiropyran form is a rigid molecule; on the contrary, the open form is considerably more flexible due to the permitted rotation through the simple C−C bond connecting the indolic and chromene substructures. In the interior of the cages of zeolite Y, in which the molecule must occupy a little more space than that available in a single cavity,[29] however, the conformational freedom must be at least partly hindered. As a result, a cis configuration with respect to the central C−C bond of the open chain is probably retained in boundary-associated **SP**. This appears to be consistent with the tight differences observed in the peak potential of III′ between the first and successive scans, as can be seen in Table 1.

Assuming that a boundary-associated pathway is operative, these electrochemical processes IV and V can be represented as:

$$\mathbf{SP}\ (b) + M^+\ (s) + e^- \rightarrow \mathbf{SP}^{\bullet -}\ (b) + M^+\ (b) \qquad (2)$$

while processes VI and VII must correspond to:

$$\mathbf{SP}^{\bullet -}\ (b) + M^+\ (s) + e^- \rightarrow \mathbf{SP}^{2-}\ (b) + M^+\ (b) \qquad (3)$$

Interestingly, the electrochemistry of **SP@MCM** and **SP@AlMCM** in $LiClO_4$/MeCN and Et_4NClO_4/MeCN electrolytes is similar to that of **SP@Y**, with the appearance of reversible couples II/II′ and III/III′ (see Figure 2). This means that, even in these large pore size materials, some spiropyran molecules show a boundary-associated response.

3.3. Electrocatalysis of *N*,*N*,*N*′,*N*′-Tetramethylbenzidine Oxidation. The electrocatalytic effect of spiropyran-containing materials on the electrochemical oxidation of *N*,*N*,*N*′,*N*′-tetramethylbenzidine (TMB) has been studied upon attachment of such probes to PIGEs. As is shown in Figure 10, a 3 mM solution of TMB in 0.10 M Et_4NClO_4/MeCN, at a bare graphite electrode TMB, yields two well-defined reversible one-electron couples in MeCN electrolytes at equilibrium potentials (calculated as the half sum of the cathodic and anodic peak potentials) of +0.50 and +0.68 V. These electrochemical processes can be described as successive one-electron transfers to give a radical cation and a dication following a scheme typical of a number of aromatic compounds:[44,53]

$$TMB\ (s) \rightarrow TMB^{\bullet +}\ (s) + e^- \qquad (4)$$

$$TMB^{\bullet +}\ (s) \rightarrow TMB^{2+}\ (s) + e^- \qquad (5)$$

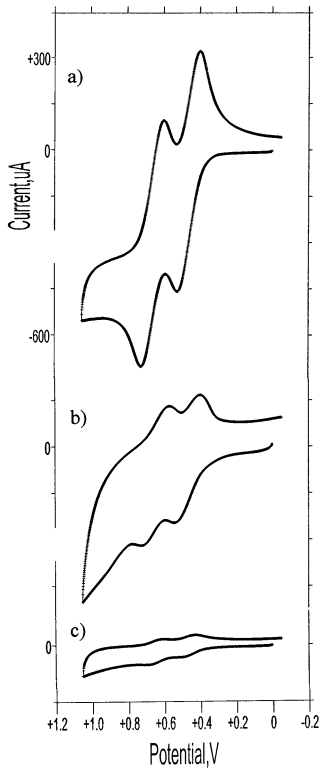

Figure 10. Electrocatalytic effect on TMB oxidation. CVs at PIGEs modified by (a) bleached **SP@Y**; (b) partly bleached **SP@Y**; and (c) pristine **SP@Y**, immersed into 3.0 mM TMB + 0.10 M Et_4NClO_4. Potential scan rate 100 mV/s.

This voltammetric pattern remains essentially unchanged for PIGEs modified by all three **SP@Y**, **SP@MCM**, and **SP@AlMCM** pristine materials in Bu_4NPF_6/MeCN, Et_4NClO_4/MeCN, and $LiClO_4$/MeCN. However, bleached materials produce enhanced currents upon immersion into Et_4NClO_4/MeCN and $LiClO_4$/MeCN electrolytes. As can be seen in Figure 10a, the peak currents of bleached **SP@Y** are significantly enhanced with respect to those obtained at partly bleached **SP@Y** (Figure 10b), which in turn are larger than those recorded for nonbleached **SP@Y** (Figure 10c). These last are almost identical to those recorded at a bare graphite electrode. These results suggest that closed spiropyran associated with the zeolite boundary is responsible for the catalytic effect. Consistently (see Supporting Information), bleached **SP@Y** does not produce any catalytic effect in Bu_4NPF_6/MeCN.

The dependence of the catalytic effect of **SP@Y**, **SP@MCM**, and **SP@AlMCM** on the electrolyte cation is illustrated in Figure 11. As can be seen in this figure, upon addition of increasing amounts of Et_4NClO_4, the peak current, i_p, recorded in CVs at sample-modified PIGES immersed into a 0.96 mM TMB + 0.10 M Bu_4NPF_6/MeCN solution, varies significantly from pristine materials to bleached materials. Thus, nonbleached materials provide peak currents that remain almost insensitive to the addition of Et_4N^+ cations. In contrast, bleached materials display currents that increase rapidly on increasing the concentration of Et_4N^+. As can be seen in Figure 12, the catalytic effect on TMB oxidation is almost exclusively from bleached **SP@Y**. Similar results were obtained upon addition of $LiClO_4$ to TMB plus Bu_4NPF_6/MeCN solutions.

As can be seen in Figure 12, although PIGEs modified with bleached **SP@Y** exhibit large peak currents, the voltammetric profile remains essentially unchanged with respect to that obtained at unmodified electrodes. The peak currents for either

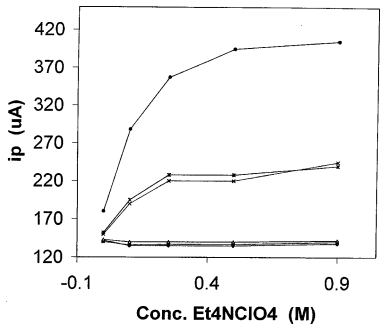

Figure 11. Catalytic effect of bleached materials on the oxidation of TMB. Dependence of the peak current on the concentration of Et_4NClO_4 for bleached **SP@Y** (points), **SP@MCM** and **SP@AlMCM** ($\times$ and stars, respectively), and pristine materials (triangles, squares, and rhombs, respectively) immersed into 0.96 mM TMB + 0.10 M Bu_4NPF_6/MeCN. From CVs at a potential scan rate of 100 mV/s.

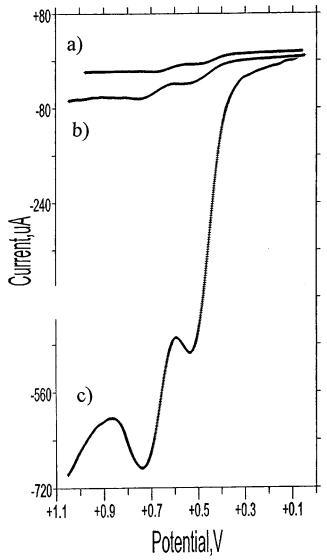

Figure 12. LSVs at (a) unmodified PIGE in 3.0 mM TMB + 0.10 M Bu_4NPF_6/MeCN; (b) **SP@MCM**-modified PIGE in 3.0 mM TMB + 0.10 M Bu_4NPF_6/MeCN; and (c) bleached **SP@Y**-modified PIGE in 3.0 mM TMB + 0.10 M Et_4NClO_4/MeCN. Potential scan rate 100 mV/s.

unmodified and **SP@Y**-modified electrodes are linearly dependent on the potential scan rate in the 10−500 mV/s range, denoting that the electrochemical process is controlled by diffusion (see Figure 13). The catalytic currents are enhanced on increasing the amount of modifier deposited on the graphite electrode between 0.10 and 0.50 mg of modifier. The following data refer to surface densities of 2.0 mg/cm^2 of modifier. No catalytic effect was observed in blank experiments performed on PFEs modified with pristine (noncontaining **SP**) zeolite Y and MCM materials.

Rotating disk voltammetry at bleached **SP@Y**-modified electrodes immersed in TMB solutions yield double s-shaped current/potential graphs. A linear dependence of the limiting currents, i_L, on the square root of the rotation rate was obtained. Accordingly, Koutecky−Levich plots (the reciprocal of the limiting current, i_L^{-1}, vs the reciprocal of square root of the rotation rate, $\omega^{-1/2}$) depicted in Figure 13 provide linear graphs. In agreement with the theory of mediated electrocatalysis,[54] this behavior corresponds to a diffusion/convection-controlled mechanism, suggesting the occurrence of relatively slow chemical reaction between the analyte and the catalytic sites which represents the rate-determining step in the overall electrode process. Here, the reciprocal of the intercept of the Koutecky−

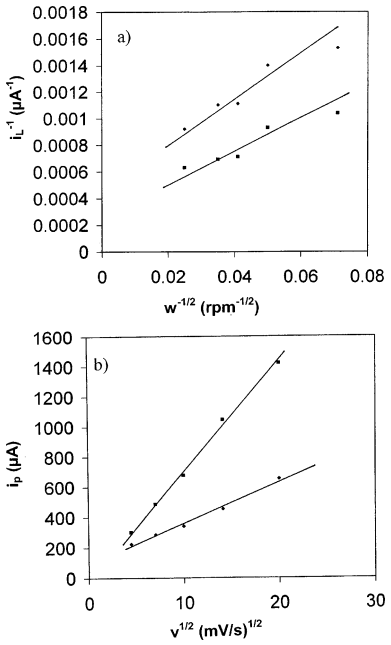

Figure 13. (a) Dependence of i_L^{-1} on $\omega^{-1/2}$ in rotating disk voltammograms recorded at a bleached **SP@Y**-modified PIGE for the first (rhombs) and second (squares) steps of TMB oxidation. (b) Dependence of i_p on $v^{1/2}$ for the first oxidation step of TMB for CVs recorded at an unmodified PIGE (rhombs) and a bleached **SP@Y**-modified PIGE (sqquares). (a) All data in 3.0 mM + 0.10 M Et_4NClO_4/MeCN.

Levich plots defines a potential-independent kinetic current, i_k, which verifies,[48]

$$i_k = nFAk\Gamma c \qquad (6)$$

where k represents a second-order rate constant, Γ is the surface concentration of catalyst present on the electrode surface, c denotes the TMB concentration in the solution, and the other symbols have their usual significance.

From the slope of the i_L^{-1} vs $\omega^{-1/2}$ representations, one can obtain the value of the rate constant, k, for the reaction between TMB and the catalyst, as described in the literature.[54] On using the effective amount of spiropyran ions determined from prior voltammetric data (1.6×10^{-10} mol/cm^2), the values of k for **SP@Y** are 2.2×10^5 and 2.6×10^5 L/(mol s), for the first and second oxidation steps of TMB in 0.10 M Et_4NClO_4/MeCN, respectively. These values are larger than those calculated for the catalysis of hydroquinone oxidation by bipyridinium ions associated with MCM-41 in aqueous medium.[36]

The fact that the electrocatalytic effect on TMB oxidation is almost exclusive of bleached **SP@Y** in $LiClO_4$/MeCN and Et_4NClO_4/MeCN electrolytes clearly suggests that only boundary-associated closed spiropyran can act as an effective catalyst for such electrochemical process. The inhibition of that electrocatalytic effect in Bu_4NPF_6/MeCN suggests, additionally, that the electron transfer is mediated to any extent by electrolyte/zeolite ion exchange.

The observed electrocatalysis can be considered as a light-driven process, controlled by irradiation of the pristine, catalytically silent material, and the site-selectivity of the boundary-associated open **SP** catalyst. This was confirmed by photochronoamperometric experiments in which a constant potential of +1.0 V was applied to **SP@Y**-modified electrodes immersed into quiescent TMB + 0.10 M Et_4NClO_4/MeCN solutions. As can be seen in Figure 14a, under dark conditions, a typical exponential decrease of the current on the time was obtained, similar to that recorded on unmodified graphite electrodes. When the

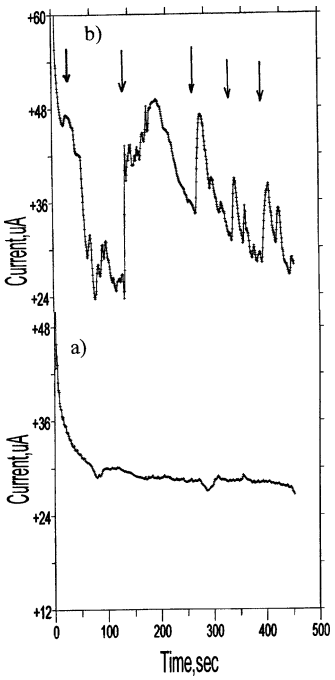

Figure 14. Current/time curves obtained upon application of a constant potential of +1.0 V to a **SP@Y**-modified PIGE immersed into a 1.0 mM solution of TMB in 0.10 M Et_4NClO_4/MeCN. The electrode was (a) maintained under dark conditions or (b) submitted to illumination with visible light during periods of 1 min (marked by arrows).

SP@Y-modified electrode was irradiated with visible light during intermittent periods of 30−60 s throughout the experiment, the current increased abruptly and decreased rapidly on ceasing the irradiation as illustrated in Figure 14b.

Because the oxidation processes of TMB take place at potentials less positive than those at which the oxidation of closed **SP@Y** occurs, the catalysis of both of the one-electron oxidations of TMB must involve the formation of a surface-confined adduct with closed spiropyran. Following the classical scheme of electrocatalytic processes, the initial reduction step of TMP (eq 4) is followed by the formation of a boundary-associated adduct:

$$TMB^{\bullet+}\,(s) + \mathbf{SP}\,(b) + M^{+}\,(b) \rightarrow [TMB^{\bullet+}\text{ --- }\mathbf{SP}]\,(b) + M^{+}\,(s) \quad (7)$$

This adduct experiences a fast dissociation that regenerates the parent $TMB^{\bullet+}$,

$$[TMB^{\bullet+}\text{ --- }\mathbf{SP}]\,(b) \rightarrow TMB\,(s) + \mathbf{SP}^{\bullet+}\,(b) \quad (8)$$

promoting a current increase in the TMB oxidation peak. To complete the catalytic cycle, the generated $\mathbf{SP}^{\bullet+}$ is electrochemically oxidized following the inverse of eq 1. A similar pathway would be applied for the second electron-transfer process.

4. Final Considerations

The voltammetry of PFEs modified with **SP@Y**, **SP@MCM**, and **SP@AlMCM** exhibits some significant differences from that of spiropyrans in MeCN solution. This electrochemistry can be rationalized on assuming the coexistence of a closed, rigid, spiropyran form, and open forms in the boundary of zeolites which are reversibly oxidized at +0.80 and +1.10 V vs AgCl/Ag, respectively, yielding radical cation species. Upon association to the zeolite (or MCM) boundary, post-electron-transfer reactions involving ring opening, cis−trans isomerization, and eventually dimerization processes occurring in the solution phase are significantly hindered, thus resulting in a reversible electrochemical behavior.

The electrochemical reduction of the parent zeolite-associated spiropyran proceeds via the nitroaromatic group in two essentially reversible one-electron steps. The reduction potentials of the electron-transfer processes for **SP@MCM** and **SP@AlMCM** are −0.85 and −1.58 V for the open forms, while the reduction of the closed spiropyran form takes place at −0.55 and −1.32 V regardless of the electrolyte media. For **SP@Y** in Et_4NClO_4 and $LiClO_4$ electrolytes, the reduction peaks are displaced ca. 100 mV toward less negative values, suggesting that a stronger association with the zeolite boundary occurs in this case.

With regard to photochemical/electrochemical processes involving the oxidation of zeolite-associated spiropyran forms, it appears that zeolite attachment stabilizes the radical cations electrochemically generated and blocks chemical reactions following electron-transfer processes, yielding an essentially reversible response for all electrode processes. This electrochemical behavior is consistent with the high photochemical reversibility observed in zeolite-associated spiropyrans, suggesting that these systems are potentially interesting as photoelectrochemical transducers.

A light-driven site-selective catalytic effect on the two-step electrochemical oxidation of TMB appears. This catalytic effect is restricted to bleached **SP@Y** in the presence of $LiClO_4$/MeCN and Et_4NClO_4/MeCN electrolytes, which is absent for that material in Bu_4NPF_6/MeCN and for all other materials in all electrolytes. Electrochemical data are consistent with the attribution of such a catalytic effect to the formation of a surface-confined adduct between closed spiropyran associated with the zeolite boundary, the rate-determining step involving the interchange of electrolyte cations. These data acr in support of the idea that boundary-associated species exhibit distinctive electrochemical properties which can be potentially interesting for selective sensing and electrosynthetic applications.

Supporting Information Available: Additional square wave and cyclic voltammograms. This material is available free of charge via the Internet at http://pubs.acs.org.

References and Notes

(1) Fischer, E.; Hirshberg, I. *J. Chem. Soc.* **1952**, 4522−4524.
(2) Guglielmetti, R. In *Photochromism, Molecules and Systems*; Durr, H., Bonas-Laurent, H., Eds.; Elsevier: Amsterdam, 1990; pp 855−878.
(3) Preigh, M. J.; Stauffer, M. T.; Lin, F.-T.; Weber, S. G. *J. Chem. Soc., Faraday Trans.* **1996**, *92*, 3991−3996.
(4) Katz, E.; Lion-Dagan, M.; Willner, I. *J. Electroanal. Chem.* **1995**, *382*, 25−31.
(5) Doron, A.; Katz, E.; Tao, G.; Willner, I. *Langmuir* **1997**, *13*, 1783−1790.
(6) Nishiyama, K.; Matsumura, K.; Fujihira, M. *Thin Solid Films* **1992**, *210−211*, 384−386.
(7) Ustamehmetoglu, B. *Polym. Adv. Technol.* **1999**, *10*, 164−168.
(8) Willner, I.; Willner, B. *J. Mater. Chem.* **1998**, *8*, 2543−2556.
(9) Campredon, M.; Giusti, G.; Guglielmetti, R.; Samat, A.; Gronchi, G.; Alberti, A.; Benaglia, M. *J. Chem. Soc., Perkin Trans. 2* **1993**, 2089−2094.
(10) Zhi, J. F.; Baba, R.; Hashimoto, K.; Fujishima, A. *J. Photochem. Photobiol., A* **1995**, *92*, 91−97.
(11) Zhi, J. F.; Baba, R.; Hashimoto, K.; Fujishima, A. *Ber. Bunsen-Ges. Phys. Chem.* **1995**, *99*, 32−39.
(12) Zhi, J. F.; Baba, R.; Hashimoto, K.; Fujishima, A. *Chem. Lett.* **1994**, 1521−1524.
(13) Mine, Y.; Ustamehmetoglu, B.; Sarac, A. S.; Mannschreck, A. *Int. J. Quantum Chem.* **1999**, *75*, 111−117.
(14) García, H.; Roth, H. D. *Chem. Rev.* **2002**, *102*, 3947−4008.
(15) Corma, A.; García, H. *Top. Catal.* **1998**, *6*, 127−140.
(16) Scaiano, J. C.; García, H. *Acc. Chem. Res.* **1998**, *31*, 783−793.

(17) Rolison, D. R. *Stud. Surf. Sci. Catal.* **1994**, *85*, 543−586.
(18) Dutta, P. K.; Ledney, M. *Progr. Inorg. Chem.* **1997**, *44*, 209−271.
(19) Baker, M. D.; Senaratne, C.; McBrien, M. *J. Phys. Chem.* **1995**, *99*, 12367.
(20) Li, J.-W.; Pfanner, K.; Calzaferri, G. *J. Phys. Chem.* **1995**, *99*, 12368−12369.
(21) Bedioui, F.; Devynck, J.; Balkus, K. J., Jr. *J. Phys. Chem. B* **1996**, *100*, 8607−8609.
(22) Senaratne, C.; Baker, M. D.; Zhang, J.; Bessel, C. A.; Rolison, D. R. *J. Phys. Chem. B* **1996**, *100*, 8610−8611.
(23) Bessel, D. A.; Rolison, D. R. *J. Phys. Chem. B* **1997**, *101*, 1148−1157.
(24) Turro, N.; Garcia-Garibay, M. In *Photochemistry in Organized Media*; Ramamurthy, V., Ed.; VCH: New York, 1991; pp 1−38.
(25) Doménech, A.; Formentín, P.; García, H.; Sabater, M. J. *J. Phys. Chem. B* **2002**, *106*, 574−582.
(26) Doménech, A.; Casades, I.; García, H. *J. Org. Chem.* **1999**, *64*, 3731−3735.
(27) Doménech, A.; García, H.; Doménech-Carbó, M. T.; Galletero, M. S. *Anal. Chem.* **2002**, *74*, 562−569.
(28) Doménech, A.; García, H.; Alvaro, M.; Carbonell, E. *J. Phys. Chem. B* **2003**, *107*, 3040−3050.
(29) Casades, I.; Constantine, M. S.; Cardin, D.; García, H.; Gilbert, A.; Márquez, F. *Tetrahedron* **2000**, *56*, 6951−6956.
(30) Casades, I.; Alvaro, M.; García, H.; Pillai, M. N. *Photochem. Photobiol. Sci.* **2002**, *1*, 219−223.
(31) Osteryoung, J.; O'Dea, J. J. In *Electroanalytical Chemistry*; Bard, A. J., Ed.; Marcel Dekker: New York, 1986; Vol. 14, p 209.
(32) Yoon, K. B.; Park, Y. S.; Kochi, J. K. *J. Am. Chem. Soc.* **1996**, *118*, 12710−12718.
(33) Sykora, M.; Kincaid, J. R.; Dutta, P. K.; Castagnola, N. B. *J. Phys. Chem. B* **1999**, *103*, 309−330.
(34) Lainé, P.; Lanz, M.; Calzaferri, G. *Inorg. Chem.* **1996**, *35*, 3514−3518.
(35) Rolison, D. R.; Bessel, D. A. *Acc. Chem. Res.* **2000**, *33*, 737−744.
(36) Doménech, A.; Alvaro, M.; Ferrer, B.; García, H. *J. Phys. Chem. B* **2003**, *107*, 12781−12788.
(37) Corma, A.; Fornés, V.; García, H.; Miranda, A.; Primo, J.; Sabater, M. J. *J. Am. Chem. Soc.* **1994**, *116*, 9767−9768.
(38) Calzaferri, G.; Lanz, M.; Li, J.-W. *J. Chem. Soc., Chem. Commun.* **1995**, 1313−1314.
(39) Scholz, F.; Meyer, B. In *Electroanalytical Chemistry, a series of advances*; Bard, A. J., Rubinstein, I., Eds.; Marcel Dekker: New York, 1998; Vol. 20, pp 1−87.
(40) Deakin, M. R.; Melroy, O. *J. Electroanal. Chem.* **1988**, *239*, 321.
(41) Bond, A. M.; Miao, W.; Raston, C. L. *J. Phys. Chem. B* **2000**, *104*, 2320−2329.
(42) Evans, J. F.; Kuwana, T. *Anal. Chem.* **1977**, *49*, 1632−1635.
(43) Engstrom, R. C.; Strasser, V. A. *Anal. Chem.* **1984**, *56*, 136−141.
(44) Perrin, C. L. In *Organic Polarography*; Zuman, P., Perrin, C. L., Eds.; Interscience: New York, 1969; p 280.
(45) Kerr, G. T. *Zeolites* **1983**, *3*, 295−297.
(46) Gemborys, H. A.; Shaw, B. R. *J. Electroanal. Chem.* **1986**, *208*, 95−107.
(47) Lovric, M.; Scholz, F. *J. Solid State Electrochem.* **1997**, *3*, 108−113.
(48) Lovric, M.; Scholz, F. *J. Solid State Electrochem.* **1999**, *3*, 172−175.
(49) Oldham, K. B. *J. Solid State Electrochem.* **1998**, *2*, 367−377.
(50) Schröder, U.; Oldham, K. B.; Myland, J. C.; Mahon, P. J.; Scholz, F. *J. Solid State Electrochem.* **2000**, *4*, 314−324.
(51) Andrieux, C. P.; Savéant, J. M. *J. Phys. Chem.* **1988**, *92*, 6761−6767.
(52) Doménech, A. *J. Phys. Chem. B*, in press.
(53) Evans, J. F.; Kuwana, T. *J. Electroanal. Chem.* **1977**, *80*, 409−416.
(54) Andrieux, C. P.; Dumas-Bouchiat, J. M.; Saveant, J. M. *J. Electroanal. Chem.* **1982**, *131*, 1−35.